Journal of Power Sources 273 (2015) 62–69

Contents lists available at ScienceDirect

Journal of Power Sources

journal homepage: www.elsevier.com/locate/jpowsour

Study of the degradation mechanisms of carbon-supported platinum fuel cells catalyst via different accelerated stress test

Yuanliang Zhang, Siguo Chen*, Yao Wang, Wei Ding, Rui Wu, Li Li, Xueqiang Qi, Zidong Wei*

Chongqing Key Laboratory of Chemical Process for Clean Energy and Resource Utilization, School of Chemistry and Chemical Engineering, Chongqing University, Chongqing, 400044, China

HIGHLIGHTS

- Three different accelerated stress test protocols were applied to investigate the Pt/C degradation mechanisms.
- The activity loss of Pt/C catalyst can be divided into recoverable activity loss and unrecoverable activity loss.
- Pt dissolution/re-deposition can be detected by using a more negative potential.
- Pt particles grow up predominantly via Pt agglomeration.
- Carbon support corrodes predominantly via the alternative decomposition formation of oxygen containing groups.

ARTICLE INFO

Article history:
Received 23 June 2014
Received in revised form
28 August 2014
Accepted 2 September 2014
Available online 16 September 2014

Keywords:
Fuel cells
Durability
Accelerated stress test
Catalyst degradation mechanism
Electrochemical impedance spectroscopy

ABSTRACT

A combination method based on three different accelerated stress test (AST) protocols along with the monitoring of electrochemical surface area (ECSA), oxygen reduction reaction (ORR) activities, X-Ray photoelectron spectrometer (XPS), transmission electron microscopy (TEM), and electrochemical impedance spectroscopy (EIS) response is introduced to investigate the degradation mechanisms of carbon-supported platinum (Pt/C) catalyst. By comparing the ECSA and ORR activity loss under different AST protocols, we revealed that the activity loss in AST can be divided into recoverable activity loss and unrecoverable activity loss. The recoverable activity loss is attributed to the reduction of Pt oxide or partially due to the removal of CO formed during carbon corrosion. The unrecoverable activity loss is ascribed to the Pt dissolution/re-deposition, agglomeration, detachment and carbon corrosion. XPS results show that the Pt dissolution/re-deposition in AST can be detected by using a more negative potential window. TEM images and analysis confirmed that the Pt growth mode in this study is mainly due to the Pt agglomeration rather than dissolution/re-deposition. EIS analysis reveals that the alternative decomposition/formation of oxygen containing groups over time is the main corrosion pathway of carbon support. These findings are very important for understanding Pt/C catalyst degradation and are also useful for developing fast test protocol for screening new durable catalyst materials.

1. Introduction

The durability of polymer electrolyte membrane fuel cells (PEMFCs) has been recently recognized as one of the most important issues to be addressed before the large scale commercialization of PEMFCs [1]. It is believed that carbon supported platinum (or platinum alloys) cathode catalysts degradation is the major failure mode for PEMFCs systems [2]. A number of mechanisms that contribute to the cathode catalyst degradation have been proposed, including Pt particle sintering, Pt dissolution/re-deposition, and carbon support corrosion [3–6]. Pt sintering was proved to be caused by the crystallite migration. Pt dissolution in PEMFCs was negligible at low and high potentials, but was remarkable at intermediate potentials. Carbon corrosion generally occurs under conditions in which the potential changes rapidly such as during continual cycling at high frequency or high oxidizing potentials are applied. Carbon corrosion from the catalyst layer causes catalyst 'wash out' and/or aggregation of support and catalyst particles.

Great progress has been achieved in this field during the past several years. However, it is still a big challenge in catalyst

* Corresponding authors. Tel.: +86 23 65105161; fax: +86 23 65102531.
E-mail addresses: csg810519@126.com (S. Chen), zdwei@cqu.edu.cn (Z. Wei).

http://dx.doi.org/10.1016/j.jpowsour.2014.09.012
0378-7753/

durability studies because the investigation of durability in PEMFCs is a time-consuming and complex task [7]. Thus, testing methods that enable more rapid screening of individual components to determine their durability characteristics are needed for evaluating catalyst durability with a rapid turn-around time. The U.S. Department of Energy (DOE) has suggested AST protocols for use in evaluating components durability and performance of electrocatalysts and supports, membranes, and membrane electrode assemblies (MEAs) [8]. While the performance of a PEM fuel cell or stack is affected by many internal and external factors, such as fuel cell design and assembly, degradation of materials, operational conditions, and impurities or contaminants [5]. It is difficult to accurately evaluate the performance and stability of the catalyst in a real fuel cell operating conditions. Electrochemically forced aging under simulated cell conditions is often carried out in a three-electrode half-cell system, in which aqueous acid solution is used to mimic Nafion [6,9]. Gasteiger and co-workers [10,11] proposed the following two test methods as reliable and efficient screening tools for fuel cell catalyst development: (i) catalyst voltage cycling test; (ii) support corrosion test at 1.2 V. They found that Pt ECSA decreased faster during potential cycling, which is also more closely related to drive cycle operation of PEMFCs on vehicles [11], than during constant potential or constant current testing. Borup et al. [12,13] have also reported potential cycling as an accelerated testing method for electrocatalysts. The loss of Pt ECSA can be used to evaluate the platinum loss caused by platinum particle sintering, platinum dissolution/re-deposition, and carbon support corrosion. Up to now, several different CV potential windows, for example, 0~1.2 V [14], 0.6~1.0 V [15], 0.6~1.1 V [2,16], and 0~1.4 V [17], have been employed to evaluate the catalyst durability. However, single CV potential window as a durability testing protocol could not distinguish the overlap degradation mechanisms induced Pt ECSA loss and it is difficult to evaluate the stability of the catalyst accurately and roundly.

In this work, we reported a combination method for examining catalyst degradation mechanisms under different potential windows. The aim of the present study is to distinguish the overlap degradation mechanisms induced Pt ECSA loss and investigate the degradation process of the Pt/C catalyst under different potential windows. To do this, three different AST potential windows were used: (1) potential cycling between 0.6 and 1.2 V in a N_2-purged 0.1 M $HClO_4$ for 4000 cycles; (2) potential cycling between 0 and 1.2 V in a N_2-purged 0.1 M $HClO_4$ for 2000 cycles; (3) constant potential at 1.5 V in a N_2-purged 0.1 M $HClO_4$ for 26.67 h. The effect of different potential windows on Pt ECSA, ORR activity, catalyst surface composition and morphology, and carbon corrosion were monitored by cyclic voltammetry (CV), ORR half-wave, X-Ray Photoelectron Spectrometer (XPS), transmission electron microscopy (TEM), and EIS.

2. Experimental

2.1. Electrode preparation

The working electrodes were prepared by applying the catalyst ink onto glassy carbon disk electrode (GC electrode, 5 mm in diameter, PINE: AFEST050GC). In summary, 5 mm diameter GC disk electrodes, which were polished to a mirror finish before each experiment (0.05 μm alumina), were used as substrates for the catalysis. For the electrode preparation, 2 mg Pt/C catalyst (40% Pt/C, Johnson-Matthey) was dispersed in 0.8 mL ethanol and sonicated for 15 min to form a uniform catalyst ink and 10 μL of this ink was pipetted onto the GC disk. After the solvent was evaporated, the deposited catalyst was covered with a drop of dilute aqueous 0.1 wt % Nafion solution; the resulting thin film was strong enough to attach the catalysts particles permanently to the GC RDE without producing any resistance. The prepared electrodes were dried at room temperature for 20 min before electrochemical tests.

2.2. Accelerated stress test (AST) and evaluation protocols

The AST experiments were performed in a standard three-electrode cell at 25 ± 1 °C temperature. The cell consisted of a glassy carbon working electrode, an Ag/AgCl (3 M KCl) reference electrode, and a Pt wire counter electrode. All potentials in this study were reported relative to the reversible hydrogen electrode (RHE). The CV and LSV electrochemical measurements were performed using an autolab PGSYAT302 instrument (IECO CHEMIE B.V., The Netherlands). The EIS was performed using a Solatron 1287 Potentiostat and a Solartron 1260 frequency response analyzer with amplitude of 10.0 mV from 10 mHz to 10 kHz. The TEM was conducted on a Zeiss LIBRA 200 FETEM instrument operating at 200 kV. The XPS was conducted on a PE PHI-5400 spectrometer equipped with a monochromatic Al X-ray source (Al KR, 1.4866 keV). Our AST protocols consisted of the following steps:

1) Before AST was commenced, the electrode was potential scanned between 0 and 1.2 V in a N_2-purged 0.1 M $HClO_4$ solution at a sweep rate of 50 mV s^{-1} for 50 cycles to obtain a steady response that defined the beginning ECSA and ORR activity. The beginning-of-life ORR activity was measured using a rotating-disk electrode operated at 1600 rpm in O_2-saturated 0.1 M $HClO_4$ solution at a sweep rate of 10 mV s^{-1}.
2) Three different AST protocols were used: (1) potential cycling between 0.6 and 1.2 V in a N_2-purged 0.1 M $HClO_4$ solution at a sweep rate of 50 mV s^{-1} for 4000 cycles; (2) potential cycling between 0 and 1.2 V in a N_2-purged 0.1 M $HClO_4$ solution at a sweep rate of 50 mV s^{-1} for 2000 cycles; (3) constant potential at 1.5 V in a N_2-purged 0.1 M $HClO_4$ solution for 26.67 h, respectively. For comparison, the total corrosion time of the three different AST methods were controlled at 26.67 h.
3) After the AST, the ORR activities of the aged-Pt/C electrode were measured using a rotating-disk electrode operated at 1600 rpm in O_2-saturated 0.1 M $HClO_4$ solution at a sweep rate of 10 mV s^{-1}. And then, the CV curves were recorded between 0 and 1.2 V in N_2-saturated 0.1 M $HClO_4$ solution at a sweep rate of 50 mV s^{-1}.
4) After CV and ORR test, the electrode were further treated with a fresh N_2-purged 0.1 M $HClO_4$ solution by cycling the potential between 0 and 1.2 V at a sweep rate of 50 mV s^{-1} for 50 cycles in order to refresh the electrode. The refreshed ORR polarization curves were measured using a rotating-disk electrode operated at 1600 rpm in O_2-saturated 0.1 M $HClO_4$ solution at a sweep rate of 10 mV s^{-1}.

The ECSA of Pt was calculated by using the following equation:

$$\mathrm{ECSA} = \frac{Q_H}{0.21 \times [\mathrm{Pt}]} \quad (1)$$

where Q_H (mC) is the charge due to the hydrogen adsorption/desorption in the hydrogen region (0.05–0.40 V) of the CVs, 0.21 mC cm^{-2} is the electrical charge associated with monolayer adsorption of hydrogen on Pt, and [Pt] is the loading of Pt on the working electrode.

3. Results and discussion

The stability of Pt/C catalyst was first investigated by potential cycling between 0.6 and 1.2 V, which caused surface oxidation/

reduction cycles of Pt. The CV and ORR polarization curves before and after AST were applied for tracking the changes of Pt/C catalyst in Pt ECSA and ORR activity over time. Fig. 1 a, A show the CV and ORR polarization curves of the Pt/C electrode before and after potential cycling between 0.6 and 1.2 V for 4000 cycles. The corresponding results are listed in Table 1. The initial Pt ECSA of the fresh-Pt/C electrode was evaluated as 61.93 $m^2\ g_{Pt}^{-1}$, compares well with other reported ECSA value for this catalyst [1]. It was found that the Pt ECSA was reduced considerably upon 4000 potential cycling between 0.6 and 1.2 V, from 61.93 $m^2\ g_{Pt}^{-1}$ to 33.74 $m^2\ g_{Pt}^{-1}$.

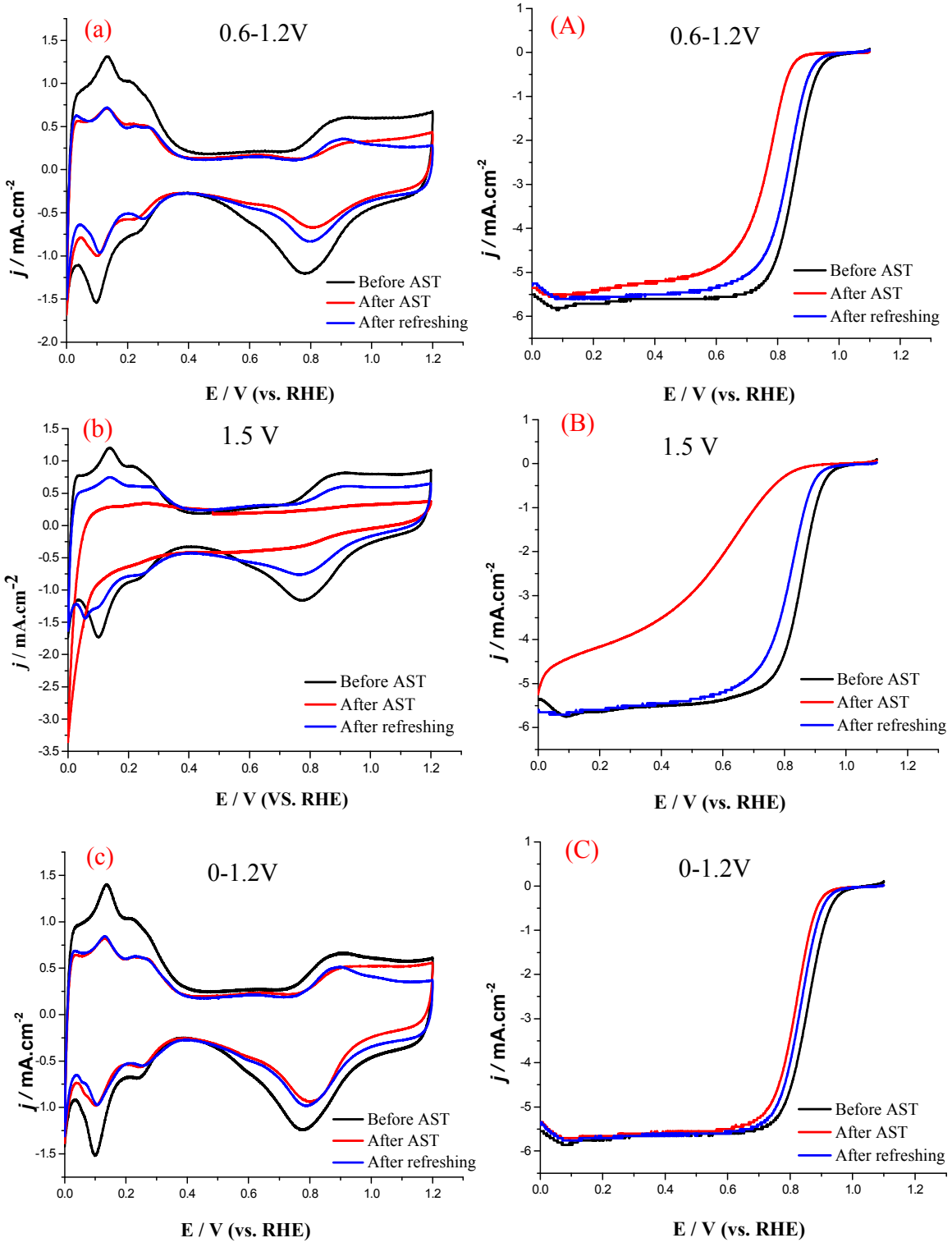

Fig. 1. CV and ORR polarization curves of the fresh-Pt/C electrodes (black), aged-Pt/C electrodes (red) by potential cycling between 0.6 and 1.2 V in a N_2-purged 0.1 M $HClO_4$ for 4000 cycles (a, A), potential cycling between 0 and 1.2 V in a N_2-purged 0.1 M $HClO_4$ for 2000 cycles (b, B), constant potential at 1.5 V in a N_2-purged 0.1 M $HClO_4$ for 26.67 h (c, C), and after further refreshed (blue) between 0 and 1.2 V in N_2-saturated 0.1 M $HClO_4$ solution for 50 cycles. (For interpretation of the references to color in this figure legend, the reader is referred to the web version of this article.)

Table 1
Electrochemical measurement of Pt/C electrodes before and after three different AST protocols.

	Before AST		After AST		After refreshing		Degradation rate		
	ESCA ($m^2\ g^{-1}$)	$E_{1/2}$ (V)	ESCA ($m^2\ g^{-1}$)	$E_{1/2}$ (V)	ESCA ($m^2\ g^{-1}$)	$E_{1/2}$ (V)	Total degradation rate (mV h^{-1})	Recoverable degradation rate (mV h^{-1})	Unrecoverable degradation rate (mV h^{-1})
0.6–1.2 V	61.38	0.8556	33.74	0.7645	34.71	0.8314	3.41	2.50	0.91
1.5 V	61.06	0.8520	/	0.5613	35.79	0.8201	10.90	9.70	1.20
0–1.2 V	61.93	0.8543	39.98	0.8158	40.01	0.8314	1.45	0.59	0.86

The ORR catalytic activity of the aged-Pt/C electrode showed 91 mV degradation in half-wave potential over the cycling period. Moreover, the formation/reduction of PtOH and PtO at potentials greater than 0.6 V shifts to higher potential, at the same time as its intensity decrease. The significant decrease in ECSA and ORR half-wave potential can be attributed to the formation of Pt oxide, Pt particle sintering, Pt dissolution/re-deposition, and carbon support corrosion. However, it is difficult to distinguish the contribution of an overlap of several different degradation mechanisms induced Pt ECSA loss and ORR half-wave potential decay. To further study the effect of different degradation pathways, the aged-Pt/C electrode was further refreshed with a fresh N_2-purged 0.1 M $HClO_4$ by cycling the potential between 0 and 1.2 V at a sweep rate of 50 mV s^{-1} for 50 cycles. It was found that the ORR half-wave potential of the refreshed-Pt/C electrode have increased 67 mV as compared with the aged-Pt/C electrode, suggesting that part of the ORR catalytic activity of the aged-Pt/C electrode can be restored. Based on above results, we can divide the activity loss into two parts: the recoverable activity loss and unrecoverable activity loss. The recoverable activity loss can be attributed to the reduction of Pt oxide or partially due to the remove of the CO formed during carbon corrosion. The unrecoverable activity loss can be attributed to the Pt dissolution/re-deposition, agglomeration, detachment and carbon corrosion. To compare the performance losses of recoverable activity and unrecoverable activity obtained in AST, the loss of ORR half-wave potential before and after refreshing is normalized with respect to its corrosion time by following equations:

$$\text{Total degradation rate}\ (\text{mV h}^{-1}) = \frac{E_{1/2-\text{Initial}} - E_{1/2-\text{AST}}}{T} \quad (2)$$

$$\text{Recoverable degradation rate}\ (\text{mV h}^{-1}) = \frac{E_{1/2-\text{Recover}} - E_{1/2-\text{AST}}}{T} \quad (3)$$

$$\text{Unrecoverable degradation rate}\ (\text{mV h}^{-1}) = \frac{E_{1/2-\text{Initial}} - E_{1/2-\text{Recover}}}{T} \quad (4)$$

where T is the total corrosion time, $E_{1/2-\text{Initial}}$,$E_{1/2-\text{AST}}$ and$E_{1/2-\text{Recover}}$ are the half-wave of the fresh-Pt/C, aged-Pt/C and refreshed-Pt/C electrodes, respectively. The corresponding results are listed in Table 1. As shown in Table 1, the calculated recoverable degradation rate under 0.6–1.2 V is 2.50 mV h^{-1}, which is much larger than the unrecoverable degradation rate 0.91 mV h^{-1}. The larger recoverable degradation rate is considered to be caused by the reduction of the Pt oxide formed at high positive potential. This assertion was further confirmed by the increase of current peak associated with the reduction of Pt oxide in the CV after refreshing between 0 and 1.2 V for 50 cycles Fig. 1a, indicating that the reduction of Pt oxide is not completely under the AST potential window 0.6 V–1.2 V.

To further study the effect of AST potential window on catalyst stability, a high positive potential and a more negative CV potential are applied: (1) constant potential of 1.5 V in a N_2-purged 0.1 M $HClO_4$ for 26.67 h, and (2) potential cycling between 0 and 1.2 V in a N_2-purged 0.1 M $HClO_4$ for 2000 cycles. Fig. 1b,B shows the CV and ORR polarization curves of the Pt/C catalyst before and after constant potential at 1.5 V for 26.67 h and further refreshed by cycling the potential between 0 and 1.2 V at a sweep rate of 50 mV s^{-1} for 50 cycles. As shown in Fig. 1 b, B, after constant potential at 1.5 V for 26.67 h, the aged-Pt/C electrode had lost all of its Pt ECSA and the ORR half-wave potential had decreased to 0.5613 V. The calculated total degradation rate is 10.90 mV h^{-1}, which is much larger than the total degradation rate 3.41 mV h^{-1} for potential cycling between 0.6 and 1.2 V. However, after refreshing between 0 and 1.2 V for 50 CV cycles, the refreshed-Pt/C electrode showed significantly increased in Pt ECSA from 0 to 35.79 $m^2\ g_{Pt}^{-1}$ and ORR half-wave potential from 0.5613 V to 0.8201 V, respectively. Moreover, the disappeared Pt oxidation/reduction peak re-appeared, at the same time as its intensity significant increased Fig. 1b, further confirmed that the formation of Pt oxide is one of the most important issues that affect catalyst activity. The calculated recoverable degradation rate is 9.70 mV h^{-1}, which is much larger than the unrecoverable degradation rate 1.20 mV h^{-1}, suggested that a high AST potential is conducive to the formation of Pt oxide.

In contrast to the significant increase in ECSA and ORR half-wave potential after refreshing between 0 and 1.2 V for 50 CV cycles, the ECSA of the refreshed-Pt/C electrode almost had no change and the ORR activity of the refreshed-Pt/C electrode only increased 16mv as compared with the aged-Pt/C electrode between 0 and 1.2 V for 2000 CV cycles Fig. 1c,C. The calculated recoverable degradation rate is 0.59 mV h^{-1}, which is much smaller than 2.50 mV h^{-1} for potential cycling between 0.6 and 1.2 V and 9.70 mV h^{-1} for constant potential 1.5 V. It is noted that the same potential cycling window between 0 and 1.2 V for aging Pt/C electrode and

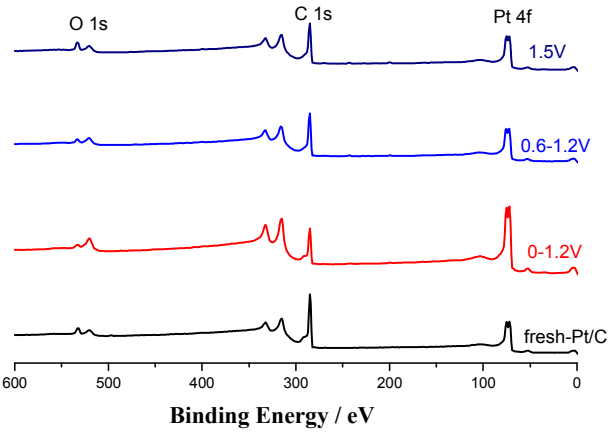

Fig. 2. XPS surveys of Pt/C electrode before and after three different AST protocols.

refreshing the aged-Pt/C electrode was used. The difference is that a fresh N_2-purged 0.1 M $HClO_4$ solution was replaced in refreshing the aged-Pt/C electrode. The CV before and after refreshing between 0 and 1.2 V for 50 cycles also show that the current peak associated with the reduction of Pt oxide almost has no any change, suggesting that the Pt surface of the aged-Pt/C electrode is metallic Pt. In this case, we can deduce that the restored ORR half-wave potential for the aged-Pt/C electrode obtained by potential cycling between 0 and 1.2 V is caused by the remove of the CO_{surf} formed during carbon corrosion [18].

The surface composition and electronic state of the Pt/C before and after three AST were also examined by XPS. Fig. 2 shows the survey spectra of the Pt/C electrode before and after three AST protocols. The corresponding results are listed in Table 2. As shown in Table 2, a significant increase in the amount of surface Pt content from 4.88% to 14.45% was observed on the aged-Pt/C electrode obtained by potential cycling between 0 and 1.2 V for 2000 cycles. The significant increase in surface Pt content can be attributed to the re-deposition of the dissolved platinum ions on the electrode surface of other platinum particles (Ostwald ripening), where metallic platinum reprecipitates through reduction of the platinum ions. In contrast to the significant increase in surface Pt content, the Pt/C electrode aged by potential cycling between 0.6 and 1.2 V and constant potential 1.5 V only show a slightly increase from 4.88% to 6.80% and 6.45%, respectively. The slightly increase in surface Pt content can be attributed to the high AST potential windows (0.6–1.2 V and 1.5 V), in which the dissolved platinum ions cannot be re-deposited on the Pt/C electrode surface. This result suggested that the Pt dissolution/re-deposition (Ostwald ripening) degradation mechanism can be distinguished by using a more negative AST potential (0~1.2 V).

Although the electrochemical experiment above provides important quantitative information about the macroscopic progress of the catalyst deterioration under different AST conditions, it does not aid in understanding the degradation mechanisms on the nanoscale. Therefore, TEM is employed to gain more insight into the reasons for the Pt ECSA and ORR activity loss. Fig. 3 a–d show the TEM images of Pt/C catalyst before and after three different AST. It can be observed from Fig. 3 A that, as expected, Pt nanoparticles in original Pt/C sample have a narrow size distribution with an average size of 3.4 nm. After AST, the structural changes are a clear sign of catalyst degradation that has taken place, as was expected from the electrochemical measurements. Most remarkably, an overlap of several different degradation mechanisms can be clearly observed in three aged-Pt/C electrodes Fig. 3 b–d: (1) the red cycles (in web version) draw attention to particles that decreased in size due to the dissolution of platinum particles; (2) the green cycles point out particles that increased in particle size due to agglomeration and Ostwald ripening; (3) the white cycle show that some Pt particles were missing completely due to the detachment of Pt particles from carbon support. A more careful examination of TEM micrographs and histogram data Fig. 3B–D revealed that the size distributions of Pt particles on the three aged-Pt/C electrodes exhibit a tail at large Pt particle sizes. According to the basis of the change in particle size distribution theory [6,19]: a particle size distribution with a tail toward small particle sizes is considered as typical for dissolution/re-deposition (Ostwald ripening) mechanism, whereas a tail toward large particle sizes is characteristic for agglomeration. Our observation in size distributions suggests that the platinum growth mode in this study is mainly due to agglomeration rather than dissolution/re-deposition (Ostwald ripening). This finding is consistent with the previous studies of Meier et al. [20] in identical location transmission electron microscopy (IL-TEM) images of aged Pt/Vulcan catalyst, where the particle growth observed mainly attributed to agglomeration. This result is somewhat contradictory with the TEM and XPS results, in which Pt dissolution/re-deposition (Ostwald ripening) can be detected. Therefore, it cannot be excluded that a dissolution/re-deposition (Ostwald ripening) mechanism is acting. In TEM study, only very small amounts of catalyst can be deposited on a TEM grid to avoid overlapping of catalyst agglomerates in the images. Therefore, the amount of dissolved Pt species is much lower than expected in a fuel cell.

Although the TEM images provide direct observation of the catalyst deterioration mechanism on the nanoscale, it is still a challenge to investigate the carbon support corrosion degradation mechanism by TEM. The structure of the overall catalyst layer is formed by many Pt/C catalyst aggregates containing primary carbon particles. The carbon particles corrosion may result in changes in the interfacial electrical properties of electrode surfaces such as resistance and capacitance, which can be detected by electrochemical impedance spectroscopy (EIS). There, EIS response is employed to monitor the resistance and capacitance change of Pt/C electrode over time and gain more insight into the carbon support corrosion mechanism. Fig. 4 a–c show the corresponding EIS Nyquist plots of Pt/C electrodes collected at different corrosion time at an open circuit potential in 0.1 M $HClO_4$ solution. The high frequency part represents the charge transfer process, protons in this case [17]. From the Nyquist plots in Fig. a–c, we can see that there is a slight change in charge transfer process and ionic resistance profile at high frequency part. This change in charge transfer process and ionic resistivity can be better visualized through Bode plots. Fig. 4d–f shows the bode plots of Pt/C electrodes under different corrosion time at high frequency region. A plot of total resistance ($R_{\sum}$) at 1584.9 Hz as a function of corrosion time is shown in Fig. 4g–i. From these we can see that the $R_{\sum}$ of Pt/C electrode showed a trend of periodic change over time, which can be attributed to the decomposition/formation of oxygen containing groups (e.g., carboxyl, carbonyl, hydroxyl, phenol, etc.) on carbon support surface under oxidative conditions [4,21]. The decrease of $R_{\sum}$ can be attributed to the decomposition of oxygen containing groups, while the increase of $R_{\sum}$ can be ascribed to the formation of oxygen containing groups under oxidative conditions over time. Such an alternating decomposition/formation process of oxygen containing groups over time will lead to the periodic change of $R_{\sum}$. This finding is consistent with previous studies that the decomposition/formation of oxygen containing groups is the major pathway of carbon support corrosion [4,5]. In terms of general application of EIS into AST, the monitoring of EIS response of Pt/C electrode over time can be used to diagnosis the degradation mechanism of carbon corrosion.

Table 2
A comparison of surface elemental compositions (atomic %) of Pt/C electrodes before and after three different AST protocols.

Samples	C1s	Pt4f	O1s
Pt/C	89.36	4.88	5.76
0–1.2 V	82.88	14.45	2.67
0.6–1.2 V	90.74	6.80	2.46
1.5 V	86.09	6.45	7.46

4. Conclusions

A combination method based on three different AST protocols along with the monitoring of ECSA, ORR activities, catalyst surface composition and morphology, and EIS response is introduced to investigate the degradation mechanisms of Pt/C catalyst. By monitoring the Pt ECSA and ORR activity loss under different AST

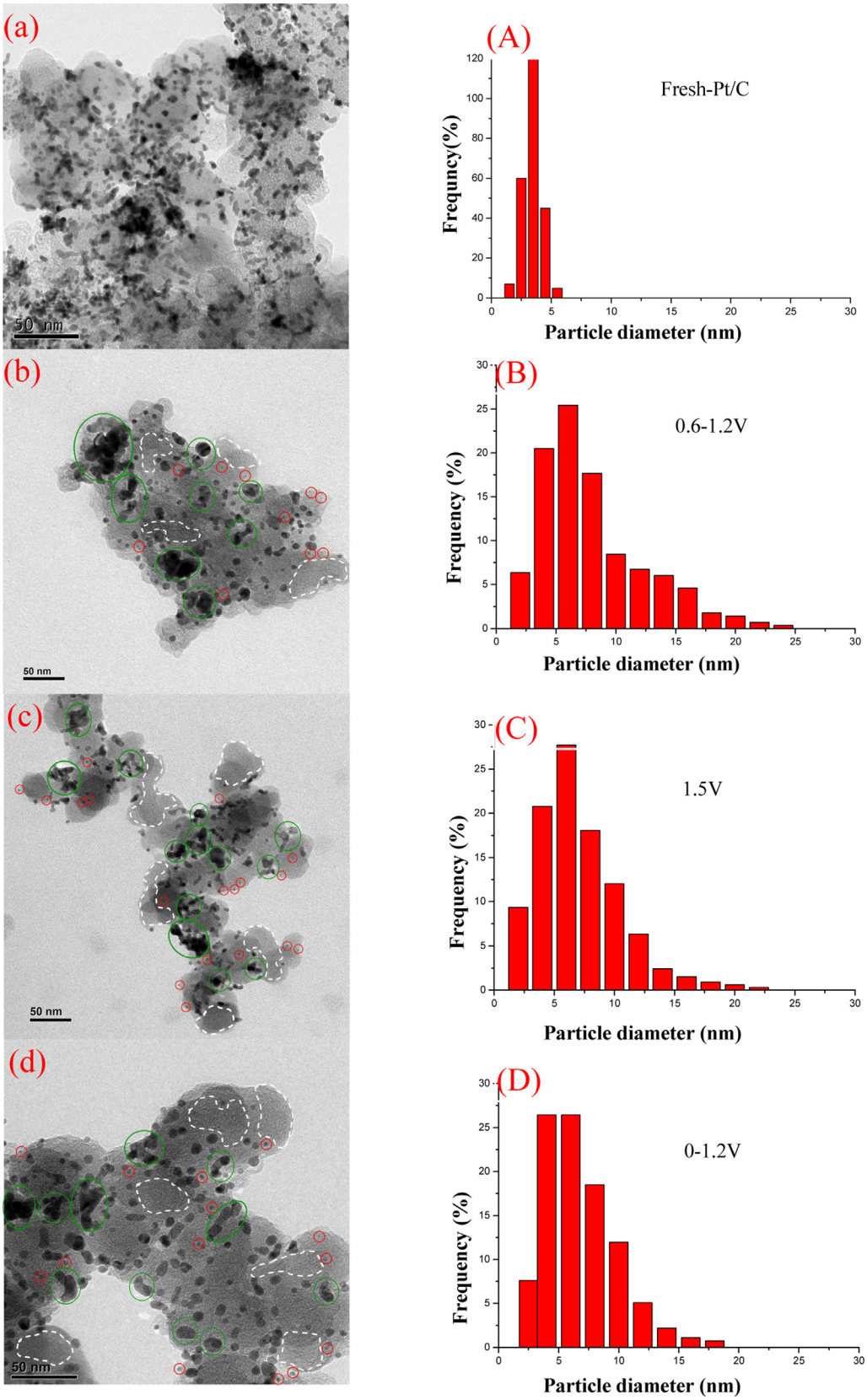

Fig. 3. TEM images and Pt particle-distribution histograms of (a, A) fresh Pt/C catalyst, (b, B) aged-Pt/C catalyst by potential cycling between 0.6 and 1.2 V for 4000 cycles, (c, C) aged-Pt/C catalyst by constant potential at 1.5 V for 26.67 h, (d, D) aged-Pt/C catalyst by potential cycling between 0 and 1.2 V for 2000 cycles.

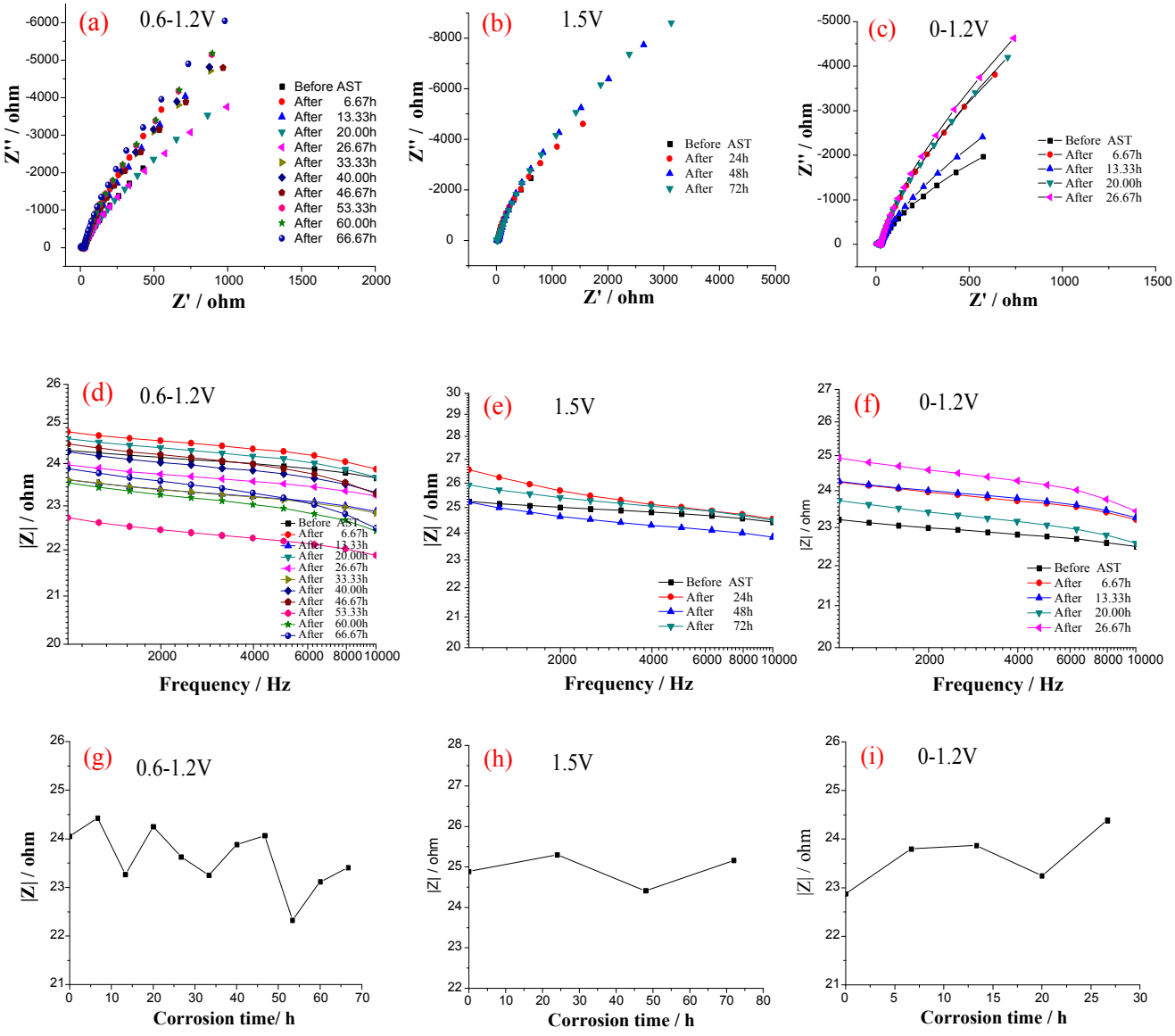

Fig. 4. Nyquist plots and bode plots and corresponding total resistance at 1584.9 Hz of Pt/C electrodes as a function of corrosion time at an open circuit potential in 0.1 M $HClO_4$ solution.

protocols, we found that the formation of Pt oxide is one of the most important issues that affect the long-term stability of Pt/C catalyst. The activity loss can be divided into the recoverable activity loss and unrecoverable activity loss. The recoverable activity loss is attributed to the reduction of Pt oxide or partially due to the remove of the CO formed during carbon corrosion. The unrecoverable activity loss can be attributed to the Pt dissolution/re-deposition, agglomeration, detachment and carbon corrosion. XPS results show that the Pt dissolution/re-deposition in AST can be detected by using a more negative potential (0–1.2 V). TEM images and analysis confirmed that the Pt growth mode in this study is mainly due to the Pt agglomeration rather than dissolution/re-deposition. By monitoring the EIS response of Pt/C electrode under different potential windows, we have shown how changes of Pt/C electrode with EIS response over time can be used to clearly identify the carbon corrosion mechanisms that are occurring. It is therefore recommended that this simple, time-efficient and reliable test protocol be more widely employed for screening new and existing catalyst layers for PEM fuel cells.

Acknowledgments

This work was financially supported by the China National 973 Program (2012CB215500 and 2012CB720300), and by the NSFC of China (Grant Nos. 21176327 and 21276291), and by the Fundamental Research Funds for the Central Universities (CQDXWL-2012-020), and by Chongqing City Fundamental and Advanced Research Program (cstc2013jcyjA90005).

References

[1] H.A. Gasteiger, S.S. Kocha, B. Sompalli, F.T. Wagner, Appl. Catal. B-Environ 56 (2005) 9–35.
[2] J. Zhang, K. Sasaki, E. Sutter, R.R. Adzic, Science 315 (2007) 220–222.
[3] X.W. Yu, S.Y. Ye, J. Power Sources 172 (2007) 145–154.
[4] Y.Y. Shao, G.P. Yin, Y.Z. Gao, J. Power Sources 171 (2007) 558–566.
[5] R. Borup, J. Meyers, B. Pivovar, Y.S. Kim, R. Mukundan, N. Garland, D. Myers, M. Wilson, F. Garzon, D. Wood, P. Zelenay, K. More, K. Stroh, T. Zawodzinski, J. Boncella, J.E. McGrath, M. Inaba, K. Miyatake, M. Hori, K. Ota, Z. Ogumi, S. Miyata, A. Nishikata, Z. Siroma, Y. Uchimoto, K. Yasuda, K.I. Kimijima, N. Iwashita, Chem. Rev. 107 (2007) 3904–3951.

[6] P.J. Ferreira, G.J. la O', Y. Shao-Horn, D. Morgan, R. Makharia, S. Kocha, H.A. Gasteiger, J. Electrochem. Soc. 152 (2005) A2256–A2271.
[7] J. Xie, D.L. Wood, D.M. Wayne, T.A. Zawodzinski, P. Atanassov, R.L. Borup, J. Electrochem. Soc. 152 (2005) A104–A113.
[8] U.S. DOE, Cell Component Accelerated Stress Test Protocols for PEM Fuel Cell, 2007.
[9] H.R. Colon-Mercado, H. Kim, B.N. Popov, Electrochem. Commun. 6 (2004) 795–799.
[10] M.F.M. Mathias, H.A. Gasteiger, J.J. Conley, T.J. Fuller, C.J. Gittleman, S.S. Kocha, D.P. Miller, C.K. Mittelsteadt, T. Xie, S.G. Yan, P.T. Yu, Electrochem. Soc. Interface 3 (2005) 24–35.
[11] R. Makharia, S. Kocha, P. Yu, M.A. Sweikart, W. Gu, F. Wagner, H.A. Gasteiger, ECS Trans. 1 (2006) 3–18.
[12] R.L. Borup, J.R. Davey, F.H. Garzon, D.L. Wood, M.A. Inbody, J. Power Sources 163 (2006) 76–81.
[13] R. Borup, J. Davey, D. Wood, F. Garzon, M. Inbody, DOE Hydrogen Program, FY 2005 Progress Report, 2005, pp. 1039–1045.
[14] S.G. Chen, Z.D. Wei, X.Q. Qi, L.C. Dong, Y.G. Guo, L.J. Wan, Z.G. Shao, L. Li, J. Am. Chem. Soc. 134 (2012) 13252–13255.
[15] M.K. Carpenter, T.E. Moylan, R.S. Kukreja, M.H. Atwan, M.M. Tessema, J. Am. Chem. Soc. 134 (2012) 8535–8542.
[16] X. Wang, W.Z. Li, Z.W. Chen, M. Waje, Y.S. Yan, J. Power Sources 158 (2006) 154–159.
[17] F.S. Saleh, E.B. Easton, J. Electrochem. Soc. 159 (2012) B546–B553.
[18] J. Willsau, J. Heitbaum, J. Electroanal. Chem. 161 (1984) 93.
[19] H.Y. Shao, P.J. Ferreira, G.J. la O', D. Morgan, H.A. Gasteiger, R. Makharia, ECS Trans. 1 (2006) 185–195.
[20] J.C. Meier, C. Galeano, I. Katsounaros, A.A. Topalov, A. Kostka, F. Schuth, K.J.J. Mayrhofer, Acs Catal. 2 (2012) 832–843.
[21] K.H. Kangasniemi, D.A. Condit, T.D. Jarvi, J. Electrochem. Soc. 151 (2004) E125.